united nations
educational, scientific
and cultural
organization

international atomic
energy agency

the
abdus salam
international centre for theoretical physics

SMR 1331/28

AUTUMN COLLEGE ON PLASMA PHYSICS

8 October - 2 November 2001

Active Galactic Nuclei: Accretion Disks and Jets - II

A. Ferrari

University of Torino, Italy

These are preliminary lecture notes, intended only for distribution to participants.

Proceedings of the International School of Physics "Enrico Fermi"
Course CXLII, B. Coppi, A. Ferrari and E. Sindoni (Eds.)
IOS Press, Amsterdam 2000

Active galactic nuclei. Accretion disks and jets. II

A. FERRARI

Università di Torino e Laboratorio Astronomico di Torino - Torino, Italy

1. – Introduction

AGNs show a strong dynamical activity originating from their cores that in radio galaxies take the form of collimated continuous jets. The same maximum powers are estimated for the radiative luminosities of AGNs and the kinetic luminosities of jets. In the so-called superluminal sources proper motions with apparent velocities larger than the velocity of light are measured by VLBI techniques. In addition the high-energy spectral components of powerful AGNs indicate Compton or self-Compton reprocessing of radiation by relativistic electrons and in the class of blazars a Doppler boosting factor is required to match the rapid variability time scales.

The observational properties of jets are summarized in the table I below.

Even before gathering morphological evidences and measuring proper motions on parsec scales, the idea of collimated continuous outflows was proposed in order to explain the energetics of extended radio galaxies [1-3]. In fact the ejection of single plasmons of scale R over distances $D \gg R$ appears unlikely on energetic grounds. The dynamical

TABLE I.

Luminosities	10^{39}–10^{47} erg s^{-1}
Variability time scales	hours to years
Jet extensions	from $\ll 1$ pc to few Mpc
Lorentz factors	≤ 20

stopping distance D is $\rho_{\rm pl} R^3 \sim \rho_{\rm amb} R^2 D$, *i.e.* $D \sim R \frac{\rho_{\rm pl}}{\rho_{\rm amb}}$, and requires $\rho_{\rm pl} \gg \rho_{\rm amb}$ and a very large momentum/energy release in a single ejection, $E_{\rm kin} > 10^{62}$ ergs, meanwhile observations suggest $\rho_{\rm pl} \leq \rho_{\rm amb}$. A continuous outflow dilutes the energy requirement over the source lifetime, that cannot be shorter than 10^7 y given the distance of radio lobes from the central AGNs. As a consequence, the jet aspect ratio is the result of the flow motion along the axis and expansion at the sound speed $\phi \sim R/D \sim a_{\rm s}/v_{\rm flow}$: this suggests supersonic speeds to comply with observed collimation and confinement.

Jet emission is non-thermal incoherent synchrotron radiation and the extension of jets requires *in situ* re-acceleration of relativistic electrons emitting at a frequency ν as

$$\tau_{\rm sync} \sim 5 \times 10^8 B_G^{-3/2} \nu_{\rm MHz}^{-1/2} \ {\rm s} < \tau_{\rm dyn} \sim \frac{D}{v_{\rm flow}} \sim 10^{14} \frac{c}{v_{\rm flow}} D_{\rm Mpc} \ {\rm s}.$$

Finally, the short-term variability and astonishingly large emission in gamma rays of associated AGNs suggests a Doppler beaming effect in inhomogeneously expanding shells/blobs of emitting relativistic electrons. The apparent quantities are related to the source characteristics by the well-known expressions

$$\tau_{\rm app} \sim \gamma^{-1} (1 - \beta \cos\theta)^{-1} \tau_{\rm source}, \qquad \nu_{\rm app} \sim \gamma (1 - \beta \cos\theta) \nu_{\rm source},$$

$$S_{\nu,{\rm app}} \sim \gamma^3 (1 - \beta \cos\theta)^3 S_{\nu,{\rm source}},$$

$$\beta_{\rm app} \sim \frac{\sin\theta}{(1 - \beta \cos\theta)} \beta_{\rm source} \quad \text{maximum at} \longrightarrow \gamma \beta_{\rm source}.$$

Under the assumption that non-thermal incoherent synchrotron emission is produced in equipartition conditions between magnetic fields and relativistic electrons [4], the basic physical parameters of jets can be estimated as in table II.

The confinement of jets on large scales where jets are no longer relativistic is either due to magnetic fields wrapped around jets or to the thermal pressure of the surrounding

TABLE II.

	Core	Jet	Hot spot	Lobe
D kpc	$\leq 10^{-3}$	2–10^3	5	50–10^3
B_{eq} gauss	—	$\leq 10^{-3}$	10^{-3}	10^{-5}
$n_{\rm e,rel}$ cm^{-3}	—	$\leq 10^{-2}$	$\leq 10^{-2}$	$\leq 10^{-4}$
polarization %	≤ 2	0–60	15	0–60
spectral index	~ 0	0.6	0.6	0.9
$v_{\rm flow}/c$	$\rightarrow 1$	10^{-1}	10^{-3}	10^{-3}

TABLE III.

$n_{\rm th}$	$\rm cm^{-3}$	10^{-4}–10^{-3}
T	K	2-3 $\times$ 10^7
B	gauss	$\leq 10^{-6}$–10^{-5}

medium. The environment is studied by X-ray observations of the hot gas surrounding active galaxies (table III).

The directly detectable physical components of jets are relativistic electrons and magnetic fields. However the stability of flows over long time scales suggests the presence of a massive component, namely protons, in the same proportion, and this fact makes the energy budget for the ejection of jets more severe. Several authors have therefore investigated the stability and propagation of relativistic positron/electron plasmas, but again the relativistic boosting factor enhances the power requirements. Another possibility is that part of or all the energy is carried by an electromagnetic Poynting flux and released into relativistic electrons along the way from the central core to the extended lobes. Some of these solutions will be commented upon in the following.

2. – Unified models for AGNs

Accretion disks releasing gravitational binding energy can provide powers up to $10^{47}\,\rm erg\,s^{-1}$ by sub-Eddington accretion rate $\dot{M} \approx 2\eta^{-1} M_\odot\,\rm y^{-1}$, where η is the efficiency for conversion of rest-mass energy into radiation. This infall process must give rise not only to radiation emission at all frequencies, but also to supersonic/relativistic jets. A scheme that combines an accretion inflow with a jet outflow appears to be able to unify the morphological and radiative properties of all AGNs and more generally of all galaxies.

A classification of AGNs along this idea has been proposed according to three basic parameters [5]:

1. accretion rate/jet power;
2. jet orientation;
3. characteristics of the surrounding medium (which may be related in part to parameter 1).

As shown in fig. 1, two basic sequences derive from observations of AGNs and jets:

a) Radio-loud objects sequence (typically associated with elliptical galaxies):

- strong sources: FR II (jets perpendicular to the line of sight) $\Rightarrow$ quasar $\Rightarrow$ blazar (jets close to the line of sight);

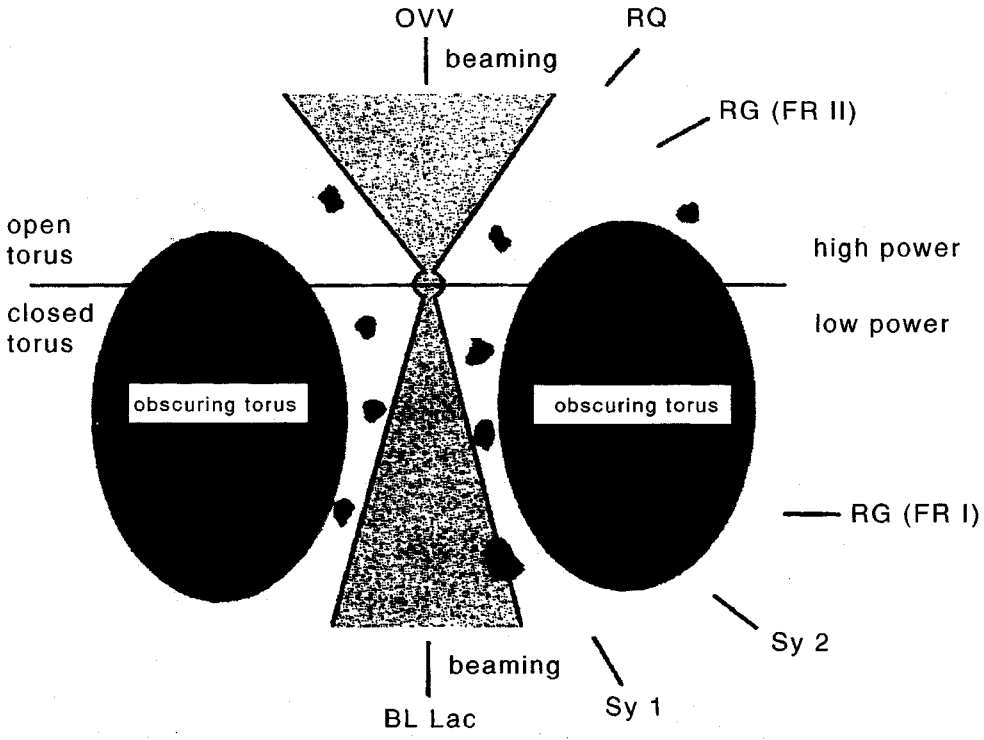

Fig. 1. – Sequences of classes in unified models of AGNs.

- weak sources: FR I (jets perpendicular to the line of sight) ⇒ BL Lacs (jets close to the line of sight).

b) Radio-weak objects sequence (typically associated with spiral galaxies):

- Sy 2 (jets perpendicular to the line of sight) ⇒ Sy 1 ⇒ radio-quiet BL Lacs (jets close to the line of sight).

The appearance of sources depends essentially on the power of the accretion disk and associated jets, separating weak and strong AGNs, and the angle of the jet direction with respect to the line of sight, separating sources with extended jets from sources in which jets act mostly through their Doppler boosting effect as they point close to the line of sight. There is also a strong influence of jets on the surrounding medium, as strong jets evacuate wider funnels of the accretion disk and in general are very straight and well ordered and end up in very clear hot spots. Weak jets appear more turbulent and fade progressively into the environment.

3. – Launching jets from accretion disks

The seminal paper on jet acceleration from accretion disks is the *twin-exhaust model* of Blandford and Rees [3]. An AGN is assumed to be surrounded by a dense, cool, rotating gas cloud in gravitational hydrostatic equilibrium; at the center of the potential well it feeds a light, hot relativistic ($\gamma = 4/3$) gas component (any accretion disk fits

in this scheme). Buoyancy forces push the relativistic gas along the least resistance direction, *i.e.* along the rotation axis, and two opposite channels are dug through the cold gas cloud.

The stationary dynamics of a 1D relativistic gas without mass losses and for isentropic flow is governed by the following mass, energy and momentum equations:

$$Q = nuA = \text{const}, \qquad L = wu\gamma cA = \text{const}, \qquad J = \left(wu^2 + p\right)A,$$

where A is the channel cross-section, $v = uc\gamma^{-1}$ the 1D flow velocity, $p = Kn^{4/3}$ the relativistic equation of state and $w = 4p$ the flow enthalpy. The solution for a flow starting from rest with stagnation pressure p_0 is

$$\frac{w\gamma}{n} = \text{const}, \qquad p = p_0\gamma^{-4},$$

$$u = \left(\gamma^2 - 1\right)^{1/2} = \left[\left(\frac{p_0}{p}\right)^{1/2} - 1\right]^{1/2},$$

$$A = \frac{1}{4}\frac{L}{c}p^{-3/4}p_0^{-1/4}\left[\left(\frac{p_0}{p}\right)^{1/2} - 1\right]^{-1/2}.$$

The flow pressure monotonically decreases outwards from p_0, u monotonically increases and the consistent channel cross-section A must decrease from infinity at p_0 to a minimum for $p_c = (4/9)p_0$ to increase again afterwards. Flow momentum is not constant but is modified by interaction at the walls:

$$Q = \frac{\left(u^2 + (1/4)\right)}{u\gamma}\frac{L}{c}.$$

At the point of minimum cross-section (nozzle point) the flow velocity is equal to the sonic velocity:

$$p_s = \frac{4}{9}p_0, \qquad A_s = 3\sqrt{3}\,\frac{L}{8p_0c},$$

$$u_s = \frac{1}{\sqrt{2}}, \qquad \gamma_s = \sqrt{\frac{3}{2}}, \qquad v_s = u_sc\gamma_s^{-1} = \frac{c}{\sqrt{3}}.$$

The radius of the channel at the nozzle can be calculated assuming equilibrium with the environment pressure, for instance $p(R) = p_0e^{-R^2/\Delta^2}$:

$$r_s = \left(\frac{A_s}{\pi}\right)^{1/2} \sim 0.5\left(\frac{L}{p_0c}\right)^{1/2},$$

$$R_s = 120\,T_8^{1/2}\left(\frac{\rho_s}{10^4 M_\odot\,\mathrm{pc}^{-3}}\right)^{-1/2}\mathrm{pc}.$$

The continuity equation

$$\nabla \cdot (\rho \mathbf{v}) = 0$$

and the z-momentum equation

$$\rho(\mathbf{v} \cdot \nabla) v_z = -\frac{\partial p}{\partial z} - \rho \frac{\partial \Phi}{\partial z} - \frac{1}{8\pi} \frac{\partial B^2}{\partial z} + \frac{1}{4\pi} (\mathbf{B} \cdot \nabla) B_z$$

together with an equation of state completely define the solution.

Blandford and Payne looked for self-similar scaling of motion and magnetic surfaces:

$$\mathbf{r} = [r_0 \xi(\chi), \phi, r_0 \chi], \qquad \mathbf{v} = \left[\xi'(\chi) f(\chi), g(\chi), f(\chi) \left(\frac{GM}{r_0} \right)^{1/2} \right],$$

i.e. all quantities scale with spherical radius along a given direction.

Neglecting thermal gas pressure in the flow (magnetically confined jets), the wind equation has the form

$$\frac{\mathrm{d}m}{\mathrm{d}\chi} = \frac{N(m, n, t, \kappa, \lambda, \xi_0')}{D(m, n, t, \kappa, \lambda, \xi_0')},$$

where $m = 4\pi\rho(v_r^2 + v_z^2)(B_r^2 + B_z^2)$ is the square of poloidal Alfvén Mach number, $n = 4\pi\rho(v_r^2 + v_z^2)/B^2$ the square of fast mode Mach number, $t = 4\pi\rho v_\theta^2 / B^2$, v_θ the speed along the spherical polar angle, $\lambda = J/(GM/r_0)^{1/2}$ and $\kappa = k(1 + \xi_0'^2)^{1/2} (GM/r_0)^{1/2} / B_0$.

Solutions are shown in fig. 2. The critical points of the system correspond to points of matching of the flow velocity with fast and Alfvén velocities ($m = 1, t = 1$). At large distances from the disk magnetic stresses are responsible for making the flow super-Alfvénic. The toroidal field B_ϕ dominates at large radii and collimates the flow into a jet.

Two classes of solutions of interest exist defined by the behavior of the fast MHD critical point:

- fast magnetosonic jets with $n \to 1$ asymptotically and paraboloidal asymptotic streamlines; 1/3 of energy is carried as bulk kinetic energy and 2/3 as Poynting flux;

- trans-fast-magnetosonic jets with $n \gg 1$ asymptotically, which focalize onto the rotation axis (this effect cannot be eliminated even when introducing thermal pressure); this class is instead dominated by the kinetic flux and in this sense is very interesting for transferring bulk energy. These solutions contain poloidal currents concentrated along the rotation axis, *i.e.* along a singular line of infinite current density; therefore a return current distributed outside the region where the jet scaling applies must be present. It must be noted that diverging current densities at large distances from the disk can produce an unstable self-pinching effect.

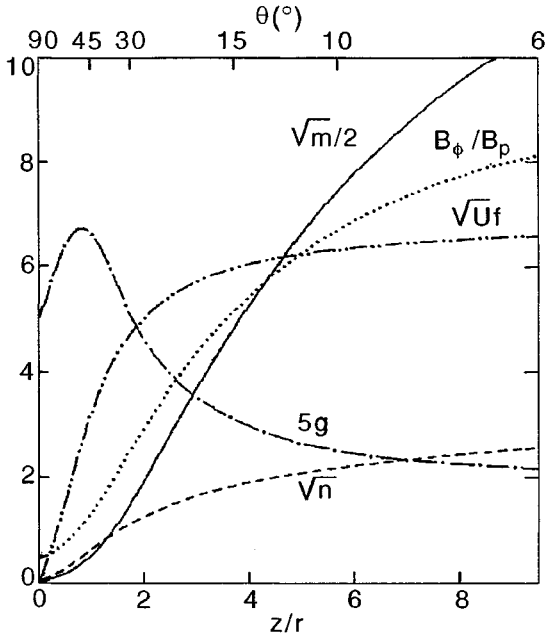

Fig. 2. – Profiles of characteristic quantities in the Blandford and Payne model of jet magneto-centrifugal acceleration.

Far from the rotation axis the flow is freely expanding and is instrumental in extracting angular momentum from the system by magnetic torque: even a small mass loss can carry a large specific angular momentum given the large lever arm.

The asymptotic flow velocity reaches at most $\sim 0.7\,c$ and cannot explain superluminal motions.

Other radial self-similar and asymptotic solutions assuming more general scaling laws have been proposed (see the review by Ferrari [5]). Here we only mention the solution by Pelletier and Pudritz [10] who analyze the 2D MHD equations for axisymmetric cold plasma outflows using a form of scaling, that does not correspond to self-similarity and does not imply complete separation of coordinates; they obtain poloidal currents that do not diverge along the rotation axis at infinity: the current is fixed and constant everywhere, giving rise to a toroidal confining field $B_\phi \propto r^{-1}$.

3·3. *Relativistic winds.* – In order to attack the question of superluminal motions Camenzind and collaborators have solved the relativistic equation for stationary axisymmetric rotating magnetized winds:

$$\alpha^2 x^2 \frac{x^2\left[\alpha^2(1-\epsilon)-M_{\mathrm{A}}^2\right]^2-\left[x^2(1-\epsilon)-\epsilon M_{\mathrm{A}}^2\right]^2}{\left(\alpha^2-M_{\mathrm{A}}^2-x^2\right)^2}\left(\frac{E}{\mu}\right)^2=\alpha^2x^4+\frac{\sigma_*^2M_{\mathrm{A}}^4}{\Phi_\psi^2},$$

where U_{p} is the poloidal 4-velocity, ψ the flux function, $\alpha^2 = -g_{tt}$ the red-shift factor from the relativistic metric, $E(\psi)$ the Bernoulli integral, $L(\psi)$ the total angular momentum constant (with magnetic stresses), μ the specific enthalpy, $x = R/R_L$, $R_L = c/\Omega$,

$\epsilon = \Omega L/E \leq 1$ a weight of the influence of magnetic energy, Φ_ψ the magnetic flux tube geometry, σ_* a dimensionless magnetization parameter.

Numerical models are summarized in Camenzind [11]: relativistic winds show the usual critical points, slow magnetosonic, Alfvénic and fast magnetosonic. Imposing that the solution goes smoothly through these points fixes three of these four parameters: for instance, one may take σ_* as a free parameter defined by the disk physics and solve for the wind equation along flux tube geometries derived from the study of the accretion flow into the disk by a Grad-Shafranov equation.

One finds that the Poynting flux carried by the flow is converted (up to $\sim 80\%$) into kinetic energy beyond R_L. The jet bulk velocity reaches Lorentz factors up to ~ 8 which is still short of the observational requirements. A wind current I is carried consistently by the flow and is determined by the total angular momentum lost through the outflow L.

3·4. *Jets from black-hole magnetospheres.* – A completely different approach to the problem of jet acceleration by disks is based on the construction of an *axisymmetric unipolar inductor* around a black hole similarly to the case of pulsars [12]. Matter inflowing with large angular momentum onto the disk carries a component B_z of magnetic field parallel to the rotation axis. Assuming a Keplerian disk, the B_z drag induces a radial electric field $E_r(r) = -(v_\phi/c)B_z(r)$ at the upper and lower surfaces of the disk. These fields are imbedded in a magnetosphere around the black hole inside the innermost stable ring of the disk and along the rotation axis. In the closed magnetosphere, $r \leq c/\omega$, $\rho\mathbf{E} + \mathbf{j} \times \mathbf{B}/c \simeq 0$. For $r > c/\omega$, charged particles loaded bend the field lines backward.

In this configuration Blandford [13] and Lovelace [14] derived the stationary solution of force-free magnetospheres and estimated the outgoing Poynting flux along the rotation axis. One can then envisage a model in which at large distances an ambient plasma absorbs the Poynting flux and gives rise to a particle jet.

In a similar context Blandford and Znajek [15], Macdonald and Thorne [16], and Phinney [17] examined the possibility of *extraction of rotational energy from Kerr black holes* by electromagnetic torques. The electrodynamics of Kerr black holes shows that they can be considered as conductors with a fixed surface electric resistance $R_H = 377\,\text{ohm}$. Thence if we consider a black hole immersed in a large scale magnetic field supported by external currents, the flux lines may thread the event horizon and originate an electric potential difference between the poles and equator, $V = \Omega_H \phi$, where ϕ is the magnetic flux threading the hole. An external circuit of plasma along magnetic lines connects pole and equator allowing an electric current to flow and dissipate at the expenses of the hole spin.

Hawking derived that the maximum energy extractable from black holes is $m - m_i \leq 0.29m$, where $m_i = (\text{horizon area}/16\pi)^{1/2} \leq (8\Omega_H^2)^{-1/2}$ is the irreducible mass for a rotating hole. This allows to calculate a current from horizon to infinity $I \sim 10^{18}\,\text{A}$ for a $10^8 M_\odot$ hole, $10^4\,\text{G}$ magnetic field, $10^{20}\,\text{V}$ potential difference. Still some uncertainties exist about the consistency of the model [18].

3·5. ADIOS *(Advection-Dominated Inflow-Outflow Solutions).* – In disks formed by ADAF the Bernoulli equation and the sound speed can be written (in the limit $v_{\rm rad} \ll \Omega r$):

$$\mathrm{Be} \equiv \frac{1}{2}\Omega^2 r^2 - \frac{GM}{r} + \frac{\gamma a^2}{\gamma - 1}, \qquad a_{\rm s}^2 = \frac{3(\gamma-1)}{5-3\gamma}\Omega^2 r^2 = \frac{6(\gamma-1)}{(9-5\gamma)}\frac{GM}{r},$$

and it can be shown that the Bernoulli constant (total energy) is positive for $\gamma < s/3$. This is not specifically linked to the scaling law assumed in ADAF, but to the fact that stationarity requires that "viscous" torques transport angular momentum and rotational energy away at some large radius where the ADAF solution becomes valid: this cannot be done by cooling (by assumption) but, for instance, by mass loss.

The ADAF configuration, although almost spherical, cannot avoid the formation of funnels along the rotation axis (inflowing gas is not supported at its base) and there any exposed gas can escape to infinity.

Blandford and Begelman [19] have found a solution that follows the self-similar scaling of ADAF ($\gamma = 5/2$), but allows for mass loss, so that accretion rate varies with r:

$$\dot{M} \propto r^p, \quad 0 < p < 1$$

and the mass lost goes into the wind. The constant inward flow of angular momentum and outward flow of energy in accretion disk are given by

$$F_l = \left(\dot{M} r^2 \Omega - G\right) = \lambda \dot{M} r^{1/2}, \quad \lambda > 0,$$

$$F_{\rm E} = G\Omega - \dot{M}\left(\frac{1}{2}\Omega^2 r^2 - \frac{GM}{r} + \frac{5a^2}{2}\right) = \frac{\epsilon \dot{M}}{r}, \quad \epsilon > 0.$$

The specific angular momentum and energy carried away by the wind are

$$\frac{\mathrm{d}F_l}{\mathrm{d}\dot{M}} = \frac{\lambda(p+1/2)r^{1/2}}{p}, \qquad \frac{\mathrm{d}F_E}{\mathrm{d}\dot{M}} = \frac{\epsilon(p-1)}{pr}.$$

The Bernoulli integral becomes, correspondingly,

$$\mathrm{Be} \equiv \frac{1}{2}\Omega^2 r^2 - \frac{GM}{r} + \frac{5a^2}{2} = pa^2 - \frac{1}{2}\Omega^2 r^2.$$

These assumptions lead to the final equation

$$\Omega r^{3/2} = \frac{(5-2p)\lambda}{15-2p} + \frac{\left[(5-2p)^2\lambda^2 + (15-2p)\left(10\epsilon + 4p - 4\epsilon p\right)\right]}{15-2p}.$$

Solutions *vs.* p, λ, ϵ can reproduce the basic characteristics of disk accretion, including Bondi accretion, ADAF and thin disks, *plus* solutions with hydrodynamic winds. For instance:

- for $p = 0$, $\lambda = 1$, $\epsilon = 1/2$ one has magnetically dominated wind with mass flow conserved in the disk; angular momentum and energy carried off with $\mathrm{d}F_{\mathrm{E}}/\mathrm{d}F_l = \Omega$; there is no dissipation, and the disk is thin and cold;
- for $\lambda = 2p[(10\epsilon + 4p - 4\epsilon p)/(2p+1)(4p^2 + 8p + 15)]^{1/2}$, the wind carries away its own angular momentum and does not exert torques on the disk.

It is not clear how these wind solutions survive the presence of magnetic coupling between disk and jets.

3˙6. *Numerical models.* – The complete study of jet acceleration from accretion disks involves highly non-linear, time-dependent phenomena. Although analytical solutions are suggestive, they are very limited: in particular only steady solutions are studied. Numerical techniques implemented on supercomputers allow today to perform interesting simulations.

Compressible hydro and magneto-hydro (fluid) models are used for simulating the supersonic jet physics (we discussed above the argument in favor of adopting fluid models). The set of compressible fluid equations is treated as a flux-conservative initial value problem:

$$\frac{\partial \mathbf{u}}{\partial t} = -\frac{\partial \mathbf{F}(\mathbf{u})}{\partial x},$$

where $\mathbf{u}$ are physical quantities and $\mathbf{F}$ is called the conserved flux. A linear system of equations is then solved by a finite difference scheme and adopting implicit or explicit algorithms with specific choices of grids.

Phenomena that have to be dealt with in compressible fluid dynamics of flows are shocks, mass entrainment, reconnection, boundary layer effects that all require a careful treatment of dissipation. The numerical treatment of dissipation defines in fact the formation of discontinuities and codes must be tested upon their capability to reproduce the real physical phenomena. We just mention the most used methods:

- *Classical methods* (*e.g.*, Lax-Wendroff, LW), adopting dissipation in linear approximation (artificial viscosity) with the same amount applied to all grid points;
- *Hybrid methods* (*e.g.*, Flux-Corrected-Transport, FCT), with non-linear numerical dissipation: high-order, less dissipative approximation in smooth regions of the flow, a low-order, more dissipative approximation at discontinuities;
- *Godunov methods* (*e.g.*, Piecewise-Parabolic-Method, PPM), based on an upwind differentiation in the direction of characteristics, introducing physical information in the numerics: cells are considered as uniform states and a standard Riemann

problem for the non-linear waves is solved across the interfaces (these methods are very robust in dealing with strong shocks);

- *Smoothed-particle hydrodynamics* (SPH), treating cells as particles interacting via collisional terms.

Concerning the reliability of numerical codes we mention that the number of spatial dimensions is crucial to follow non-linear mode coupling and formation of fluid turbulence: computations in 2D or 2.5D may largely differ from 3D. Similarly the extension of the integration domain (both in space and time) must be large enough for testing which evolutionary patterns are transient or stationary. MHD models are essential: this increases the number of characteristics in the mathematical system and makes the numerical solutions more unstable.

To estimate the final flow velocity 1D simulations are acceptable: the walls of the flow channel are fixed boundaries and provide a radiation field with a Poynting flux with a non-negligible component along the funnel's axis [7, 20]. Optically thick and thin flows can be accelerated up by radiation up to an asymptotic value $\Gamma_{\rm bulk} \sim 2$–3, fixed by Compton drag by the photon field itself. A solution to this limit has been proposed by Ghisellini *et al.* [21]: clouds of electrons in the flow can synchrotron self-absorb the radiation from the disk or funnel, absorption is selective so that red-shifted photons fall below an absorption cut-off and therefore cannot brake the flow. Lorentz factors up to $\Gamma_{\rm bulk} \sim 10$ are attained.

3·6.1. Sweeping magnetic twist. Uchida and collaborators [22, 23] solved an initial value MHD problem in 2D axisymmetric and 3D geometries by a Lax-Wendroff scheme for the case of geometrically thin disk with $(v_{\rm s}/v_{\rm K})^2 \leq 10^{-2}$ rotating around a point mass at Keplerian or sub-Keplerian azimuthal velocities ($v_\phi/v_{\rm K} = 0.6$–1.0).

Newtonian ideal MHD equations in cylindrical geometry (r, ϕ, z) are

$$\frac{\partial \rho}{\partial t} + \nabla \cdot (\rho \mathbf{v}) = 0,$$

$$\frac{\partial}{\partial t}(\rho v_r) + \nabla \cdot (\rho v_r \mathbf{v}) - \frac{\rho v_\phi^2}{r} = -A_1 \frac{\partial p}{\partial r} + \frac{A_2}{4\pi}\left[(\nabla \times \mathbf{B}) \times \mathbf{B}\right]_r + A_3 \rho g_r,$$

$$\frac{\partial}{\partial t}(\rho v_z) + \nabla \cdot (\rho v_z \mathbf{v}) = -A_1 \frac{\partial p}{\partial z} + \frac{A_2}{4\pi}\left[(\nabla \times \mathbf{B}) \times \mathbf{B}\right]_z + A_3 \rho g_z,$$

$$\frac{\partial}{\partial t}(r \rho v_\phi) + \nabla \cdot (r \rho v_\phi \mathbf{v}) = \frac{A_2}{4\pi} \nabla (r B_\phi \mathbf{B}),$$

$$\frac{\partial \mathbf{B}}{\partial t} - \nabla \times (\mathbf{v} \times \mathbf{B}) = 0,$$

$$\left(\frac{\partial}{\partial t} + \mathbf{v} \cdot \nabla\right)\left(\frac{p}{\rho^\gamma}\right) = 0$$

with $\mathbf{g} = -\nabla\Phi = \nabla(r^2 + z^2)^{-1/2}$ the effective gravity, $A_1 = v_{s0}^2/(\gamma v_{\phi 0}^2)$, $A_2 = v_{A0}^2/v_{\phi 0}^2$, $A_3 = v_{K0}^2/v_{\phi 0}^2$, $v_{s0}^2 = \gamma R T_0$ the sound speed, $v_{A0}^2 = B_0^2/(4\pi\rho_0)$ the Alfvén speed, $v_{K0}^2 = GM/r_0$ the Keplerian velocity, $v_{\phi 0}$ the rotational speed (the subscript 0 indicates quantities measured at the disk surface). The simulation starts with a uniform poloidal magnetic field penetrating the disk vertically and such that $(v_A/v_K)^2 = 10^{-2}$–10^{-3}, plus a non-rotating corona present outside the disk. The disk differential rotation bends the poloidal magnetic lines and develops a toroidal structure; the magnetic tension excess in the disk is released along poloidal lines as large-amplitude torsional Alfvén waves (*sweeping magnetic twist*). The process extracts angular momentum from the disk and this initiates a collapse toward the center. When the toroidal field has become strong enough, mass is ejected along the poloidal lines and gives rise to a hollow jet structure.

There acceleration of the jet matter is essentially due to the $\mathbf{J} \times \mathbf{B}$ and centrifugal forces, as derived in the Blandford and Payne steady model. The final magnetic configuration has a poloidal field of hourglass shape with a helical toroidal annulus moving axially at the local Alfvén speed: ejection velocities are a few times v_K.

Stone [24] used a less dissipative numerical code, the Parabolic Piecewise Method (PPM), to investigate a similar configuration but for low magnetic fields. In this case the dynamical process enhancing the disk field corresponds to the Balbus and Hawley magneto-rotational instability, which enhances the accretion rate onto the central black hole as a results of the extraction of angular momentum by the Alfvén torsional waves which in turn form jets along the rotation axis.

3·6.2. Thick accretion disks. Matsumoto *et al.* [25] investigated geometrically thick disks in axisymmetric conditions, obtaining an effect of accretion avalanche at the surface of the disks where torsional Alfvén waves accelerate jets and remove angular momentum. The outer streamlines of the accretion flows pulling the magnetic field from the upper and lower surfaces of the disk meet at the outer tip of the disk with opposite magnetic polarities: correspondingly, magnetic reconnection may take place and be used to produce non-thermal particles.

3·6.3. Stationary outflows. A set of numerical studies aims to show the existence of stationary solutions. For instance, Romanova *et al.* [26] assumed the disk as a fixed boundary with initial strong monopole magnetic field. The matter is pushed out from the disk with velocity smaller than the slow magnetosonic velocity and accelerated through the three MHD critical points reaching a super fast magnetosonic final velocity. However no collimation is possible at large distances where kinetic energy prevails, and stationary solutions do not exist for $\beta = v_s^2/v_A^2 \gg 1$ due to the formation of a strong toroidal field that pinches the outflow in a non-steady condition.

Ouyed and Pudritz [27] employed a 2.5D time-dependent code (ZEUS) for simulating disks accreting at sub-Eddington rates. Again the disk is just a fixed boundary with a cold corona above and below in stable equilibrium as supported by Alfvénic turbulent pressure (eventually generated by the Balbus and Hawley instability). The initial magnetic field configuration in the corona is poloidal by a potential field ($\mathbf{J} = 0$), smoothly connected

with a toroidal magnetic field in the disk $B_\phi \propto 1/r$. Gas is expelled from the disk into the corona at very small speed ($v_z = 10^{-3} v_K$) and magnetic lines are opened to more than the critical angle for being magneto-centrifugally accelerated. Collimation in cylindrical structures parallel to the rotation axis is produced by the pinching force of the toroidal field at asymptotic distances [28].

Stationary solutions are found for relatively strong magnetic fields, $\beta \sim 1$, at the innermost radius of the disk with the jet axial velocity a few times the Keplerian velocity at the fast magnetosonic point and then increasing $\propto z$. A large fraction of the energy in the jet is in poloidal kinetic energy (2/3 of total), the rest in toroidal magnetic energy.

Meier *et al.* [29] studied numerically the Blandford and Payne model, in the case of strong magnetic field, initially purely poloidal ($B_\phi = 0$) anchored in the disk, with lines protruding into the corona at an angle $\theta \leq 60°$ with respect to the disk. The disk is thin, cold and dense with a tenuous hot corona. The dynamical characteristics of collimated jets depend on the ratio $\nu = v_A/v_{esc}$ in the corona:

- for $\nu \leq 1$ gravitational forces dominate over magnetic forces and the jet is accelerated by an upward recoil due to an increase of the disk magnetic field by differential rotation; this acceleration has low efficiency and the final velocities are below v_{esc};
- for $\nu \geq 1$ the jet is produced by magneto-centrifugal acceleration and is collimated by an azimuthal field; the final velocities are typically $v_j \geq 10 v_{esc}$ for v_A of the order of the Keplerian velocity at the inner radius of the disk and increase further for increasing v_A.

The transition between the two modes of jets is rather sharp (*magnetic switch*), but there is no switch in total power.

For small fields the jet transports essentially magnetic energy, while for large fields a significant amount goes into kinetic energy.

In relativistic conditions the asymptotic bulk Lorentz factor of highly magnetized solutions can be as large as $\gamma \approx 10$.

3·6.4. Episodic outbursts. The brightness distribution observed in jets is very knotty, beginning from VLBI scales. In addition, short time scales variabilities in blazars are measured which may be due to irregularities in acceleration phase.

In the sweeping twist such an effect can be related to the recurrent uncoiling of the magnetic toroidal field created by the disk differential rotation propagating torsional Alfvén "bursts" along jets.

Ouyed and Pudritz [27] analyzed the influence of the magnetic topology, confirming that centrifugally driven winds are not possible if the poloidal magnetic lines are inclined by an angle $\geq 60°$ to the disk. When field lines are initially close to parallel to the rotation axis, the progressive winding of magnetic lines in the disk generates large amplitude non-linear torsional Alfvén waves similar to those predicted by Uchida and Shibata. However, as the twisting of magnetic lines increases approaching the central parts of the disk, the resulting strong gradient generated in the toroidal magnetic field opens up any vertically

uniform magnetic structure, so that the opening angle becomes $\leq 60°$. Such wind does not reach a stationary state, but is threaded by regularly spaced knots where a toroidal field tends to recollimate the flow towards the axis producing MHD shocks.

Romanova *et al.* [26] apply their code to steady flows for $\beta = v_s^2/v_A^2 \gg 1$. The outflow is pinched by a strong toroidal component in a non-steady condition, and becomes intermittent between a configuration favorable (open field lines) and unfavorable (pinched lines) to magneto-centrifugal acceleration.

4. – Jet propagation over large scales

Jets undergo a huge expansion phase at the exit from the inner core (≥ 0.1 pc): in a few parsecs their radius increases by ~ 1000 times without loosing momentum, directionality and collimation. This is in sharp contrast with laboratory experiments on both dense or light flows, where, in the case of sudden expansion into a negative pressure gradient, various types of fluid instabilities, internal shocks and turbulent entrainment disrupt the collimated propagation. However, extragalactic jets are in a largely supersonic regime for which after a nozzle the maximum bending of streamlines is fixed by the local Mach number:

$$\theta - \theta_0 \approx \frac{2}{\Gamma - 1} \frac{1}{\mathrm{M}_j},$$

i.e. in order to maintain confinement jets must be highly supersonic [30]. At the same time development of a rich internal dynamics is needed in order to interpret the observed morphologies (knots, wiggles, large scale bendings, etc.). Therefore a fine tuning of the physical parameters must take place in order to produce all these features.

4·1. *Confinement.* – Various types of confinement mechanisms have been investigated, such as ballistic, thermal, inertial, magnetic, etc. Most likely they can all be present in different phases of propagation of a jet. In particular:

- thermal confinement by external intergalactic plasma pressure is sufficient in FR I jets [31];
- inertial confinement by ram pressure in a cold ambient medium is possible in compact dense regions;
- ballistic confinement can operate on single bullets of a discontinuous jet;
- magnetic confinement by external (intergalactic) magnetic fields advected from the jet acceleration region is also quite possible, provided they are properly tuned along the jet to avoid pinching instabilities;
- magnetic-field confinement can be provided by a large scale intergalactic field corresponding to the poloidal component assumed in MHD jet acceleration models; the accreting plasma deforms the fields to an hourglass shape reaching an asymptotic cylindrical geometry outside the core [28];

- confinement by the overpressured cocoon generated by the backflow formed at the jet head and enveloping the whole structure.

4·1.1. Gas confinement. The propagation of a laminar jet confined by thermal pressure in stationary Newtonian, hydrodynamic limit for a polytropic gas $P = K\rho^{\delta}$ is governed by the mass and energy discharge conservations:

$$\rho v A = \dot{M}_j \Rightarrow P^{(\delta+1)/2\delta} \mathsf{M}_j A = \text{const},$$

$$P^{(\delta-1)/\delta}\left[\frac{\mathsf{M}_j^2}{2} + \frac{\delta/\Gamma}{\delta-1} + \frac{\Phi}{a_s^2}\right] = \text{const},$$

where M_j is the flow Mach number, Φ the gravitational potential. Assuming $\dot{M}_j$ and L_{kin}, with $\mathsf{M}_j \gg 1$ and $v = \text{const}$, one obtains

$$\mathsf{M}_j \propto P^{(1-\delta)/2\delta}, \qquad A \propto P^{-1/\delta}.$$

For the jet pressure balanced by a typical pressure profile in galaxies, $P_{\text{ext}} \propto r^{-n}$ with $n = 2$, the angle subtended by the jet width as seen from the nucleus decreases as $\theta \sim A^{1/2} r^{-1} \propto r^{(n-2\delta)/2\delta} \sim r^{-2/5}$. This shows that jets can be collimated even though their area expands.

It must be noted that the flow pattern depends also on the profile of the extended gravitational potential outside the nucleus: for adiabatic jets a mass distribution $M_{\text{gal}} \propto r^{-s}$, with $s \leq \delta$, does not allow the flow to reach a transonic point and the flow is stopped inside the galaxy [32].

4·1.2. Magnetic confinement. The basic assumption in magnetic confinement of large scales jets comes from the conclusions of the study of jet acceleration, namely that

- both poloidal B_{p} and toroidal B_ϕ magnetic components are supported by the dynamics of accretion disks and advected in the flow to large scales;
- the poloidal component actually increases the internal jet pressure and loosens collimation;
- the toroidal component pinches the flow toward the axis, possibly yielding instabilities.

Under these conditions the jet expansion causes a decay of the magnetic components as $B_{\text{p}} \propto R^{-2}$, $B_\phi \propto R^{-1}$, where R is the jet radius: this agrees qualitatively with typical observations showing the initial part of the jet dominated by longitudinal (poloidal) fields and later by the perpendicular (toroidal) component, but synchrotron luminosity does not decay as rapidly as the simple adiabatic expansion law would predict, $L \propto R^{-(5+4\alpha)}$. Magnetic flux can be added along the flow by entrainment or turbulent shear amplification or dynamo effects [33].

Quantitative analyses of the large scale structure of magnetized jets have been presented by various authors. In general, the confinement is governed by the Grad-Shafranov equation, that in relativistic form for a cold plasma is [34]

$$\left(1-\frac{R^2}{R_L^2}\right)\nabla_\perp\frac{B_p^2}{8\pi}-\frac{B_p^2R}{2\pi R_L^2}\nabla_\perp R+\frac{1}{2\pi c^2R^2}\nabla_\perp\left(\frac{cRB_\phi}{2}\right)^2=0,$$

where $cRB_\phi/2$ is the global poloidal current and $R_L=c/\Omega$.

Currents and current gradients are essential in the structure of jets dominated by self-electrodynamic forces. Collective effects in plasmas are efficient in maintaining charge neutrality, but jets may carry a net current. Self-confinement by the tension of toroidal field lines in current-carrying jets was originally proposed by Benford [35] requiring

$$I\sim 10^{17}P_{-12}^{1/2}d_{\rm kpc}\,{\rm A}\qquad (P\text{ pressure})$$

with $B_\phi\propto 1/R$. A question often asked is: how to close the electric circuit? In fact two possibilities exist for the return current:

- current at large radii closing onto the central object through the accretion flows with very low current density and low magnetic stresses in the external medium;
- current connected with the plasma backflow generated at the head of the jet, which creates a cocoon shielding the jet from external interactions.

4·2. *Jet instabilities.* – Laboratory experiments (mostly subsonic) show that collimated beams maintain their directionality for relatively short distances, typically less than 10 times their diameter, due to onset of fluid instabilities, shocks, boundary layer effects and turbulent mixing with the external medium [36]. Astrophysical supersonic and/or super-Alfvénic jets appear instead much longer lived, although they are modulated by knots, bends, internal shocks of the same type observed in the laboratory.

The most obvious type of instability is the *Kelvin-Helmholtz instability*: if a ripple develops at the interface between the two fluids in relative motion, the flow over the ripple has to be faster, and therefore, according to the Bernoulli equation, exerts less pressure and allows the ripple to grow further [37]. The linear analysis shows that two types of unstable modes exist: *ordinary surface modes*, with amplitude steeply decreasing away from the interface, and *reflected body modes*, which affect the whole plasma in the jet; body modes are typical of supersonic jets.

The most unstable wavelengths are typically

$$\lambda_{\rm KH}\sim 2\pi R{\rm M}_j$$

with growth times

$$\tau_{\rm KH}\sim\frac{1}{{\rm Im}\,\omega}\sim\kappa\frac{\lambda_{\rm KH}}{R}\tau_{\rm c};$$

$\tau_{\rm c}=2R/a_{\rm s}$ is the beam crossing time at the speed of sound, R the beam transverse scale and $\kappa\leq 0.5$ a factor depending on the specific geometry, mode and density contrast;

for magnetized modes a_s is replaced by a_A. Ordinary modes dominate for $M_j \leq 2\sqrt{2}$, reflected modes above this limit. High density in the jet and strong magnetic fields reduce the effect of instability. The critical element in the instability evolution is the physical extent of the contact layer between the jet and the ambient medium: all modes with wavelength shorter than the scale gradient are stabilized.

Time scales are rather short with respect to the propagation time scale of astrophysical jets and therefore these modes can affect them soon after the exit from the nozzle. Long wavelength modes modulate the morphology of the beam, while short wavelengths can give rise to a turbulent cascade.

Another type of interesting instability is the *filamentation instability* originating from synchrotron "thermal" runaway, where locally compressed gas radiates more and reduces the gas pressure leading to further compression. Filaments overpressured with respect to the external plasma are brighter than the surrounding medium because of enhanced emission, provided a suitable input of fresh particles is guaranteed [38].

Resistive instability can also be relevant for magnetically confined jets: reconnection modes develop in neutral sheets or shears and may lead to energy dissipation and suprathermal particle acceleration.

4·3. *Non-linear evolution of jet dynamics.* – The non-linear evolution of the jet dynamics must be studied by numerical codes. Solution of the set of Navier-Stokes or Euler plus Maxwell equations is still limited to relatively low Reynolds numbers (high viscosity) $\mathrm{Re} \leq 100$ due to the discretization process by finite difference schemes: this fact limits the possibility of understanding the detailed development of instability and turbulence. Another difficulty is to follow the evolution to very large time scales because of the limited integration domain.

The main phases of hydrodynamic simulations of jet propagation are:

Linear phase ($t \leq 10R_j/a_s$). Modes excited by an initial perturbation evolve according to the linear theory. At the end of this phase a zig-zag pattern of internal shocks (conical for cylindrical jets, oblique for slabs) forms and the pressure build-up makes the jet expand. Little energy and momentum exchange between jet and ambient is observed.

Acoustic phase ($10R_j/a_s \leq t \leq 20R_j/a_s$). The growth of deformations of the jet produces piston-like fronts that drive shocks into the external medium, leading to conspicuous energy and momentum transfer from the jet to the ambient. Light jets transfer more momentum than heavy jets.

Mixing phase ($20R_j/a_s \leq t \leq 30R_j/a_s$). At this stage light jets break up because of matter entrainment from external medium and become very turbulent; heavy jets mix vigorously with the external material.

Quasi-stationary phase ($t \geq 30R_j/a_s$). In this final phase jets reach a quasi-stationary highly turbulent configuration that depends on the density ratio. Heavy jets maintain a coherent directionality, light jets appear completely mixed and diffused.

The evolution becomes much faster in 3D simulations of cylindrical jets [39]. Mixing starts much earlier due to the more rapid growth of small scale structures, and this is particularly evident in light jets where fluting modes are present in the linear phase already

with growth rate larger than helical modes. Light jets are asymptotically disrupted by a strong transition to turbulence. Dense jets survive as collimated structures although the energy and momentum lost by entrainment is larger and the process occurs faster, over time scales $t \sim 10R_j/a_s$. The final flow velocity is also reduced and the jet cross-section is broadened, as consistent with strong mass entrainment, that can reach up to 100% of the jet mass.

In the case of non-linear MHD simulations similar effects are obtained. Non-linear simulations in current-carrying beams are not yet available. For this task it looks essential to develop two-fluid codes.

An important feature observed in all simulations is the formation of shocks in the form of conical structures inside a cylindrical jet forming a typical angle $\sim 1/\mathrm{M}_j$: the zig-zag pattern of oblique shocks is a typical feature of the non-linear evolution of jets. Shocks travel with the flow at a velocity slightly below the jet velocity, and the intersection points of shocks correspond to high-pressure regions where strong radiation emission can be expected. In later stages, due to mass entrainment and momentum diffusion, shocks extend at large distances into the external medium perpendicularly to the flow and become substantially transverse structures.

5. – Jet termination

Jets terminate in extended radio lobes where the energy transported by the continuous flow is released in the environment through complex physical processes. Morphological features of lobes are: *hot spots*, compact overpressured regions at the tips of jets, *cocoons*, extended and supersonically expanding overpressured regions, *filaments*, threading the whole region possibly as transient structures. The main questions for plasma models are:

- *Energetics*: if the plasma contains protons and electrons with identical number density, the total kinetic energy $L_j \sim 10^3 L_{\mathrm{rad}}$ [2]; an electron-positron pair plasma requires highly relativistic bulk velocities to reduce the annihilation rate and consequently large inertial masses would be necessary anyway [40].

- *Global dimensions*: much larger than the jet cross-section, and larger than expected from an expansion of the overpressured gas in the head or hot spots over the source lifetime; oscillations in the direction of the flow ejection related to some fast periodicity in the AGN (dentist drill model).

- *Stability*: the working surface is disrupted by mixing and turbulence that give rise to different types of backflows and cocoons; the cocoon itself is unstable to filamentary instabilities.

- *Radiation emission*: local particle acceleration must operate for supporting synchrotron emission, especially in hot spots and filaments; diffusion must efficiently transport particles all over the lobe.

We comment about the physics used to model extended lobes.

5·1. *Hot spot formation.* – The working surface of a jet is generally considered a termination shock and its dynamics is defined by balancing thrust and external medium ram pressure force:

$$\Pi_{\rm j} \sim \frac{L_{\rm j}}{(v_{\rm j}-v_{\rm h})} \sim \frac{\rho_{\rm j}(v_{\rm j}-v_{\rm h})^3 A_{\rm j}}{(v_{\rm j}-v_{\rm h})} = \Pi_{\rm ram} \sim \rho_{\rm e} v_{\rm h}^2 A_{\rm j},$$

where $L_{\rm j}$ is the jet's kinetic luminosity, $v_{\rm j}$ the flow velocity, $v_{\rm h}$ the head's forward velocity, $\rho_{\rm j}$ and $\rho_{\rm e}$ the jet's and ambient's velocity, respectively. Defining the density ratio $\nu = \rho_{\rm e}/\rho_{\rm j}$ one derives

$$v_{\rm h} \sim \frac{v_{\rm j}}{1+\sqrt{\nu}},$$

i.e. light jets ($\nu \gg 1$) are decelerated very early in their propagation.

5·2. *Dimension of lobes.* – The advancing jet creates a bow shock in the intergalactic medium. From the jet's head a backflow moves backwards enveloping the jet and inflates an overpressured cocoon around the whole radiogalaxy. The cocoon's *length* is determined by the balance between the jet's thrust and the ram pressure of the external medium; its *width* by the internal pressure that expands in the external medium at the sonic speed [41].

The jet kinetic pressure $L_{\rm j}/v_{\rm j}$ balances with the external gas ram pressure $\rho_{\rm e} v_{\rm h}^2 A_{\rm h}$ through the cross-section $A_{\rm h} \geq A_{\rm j}$ if the direction of jets jitters (see fig. 3):

$$L_{\rm j} \sim (\rho_{\rm e} v_{\rm h}^2 A_{\rm h}) v_{\rm j}.$$

The cocoon pressure $P_{\rm c} \sim \rho_{\rm e} v_{\rm c}^2$ drives a sideways shock into the IGM at a speed $v_{\rm c} \sim (L_{\rm j} v_{\rm j} A_{\rm h}/\rho_{\rm e})^{1/4} t^{-1/2}$ and inflates an area $A_{\rm c} \sim (L_{\rm j} v_{\rm j} A_{\rm h}/\rho_{\rm e})^{1/2} t$.

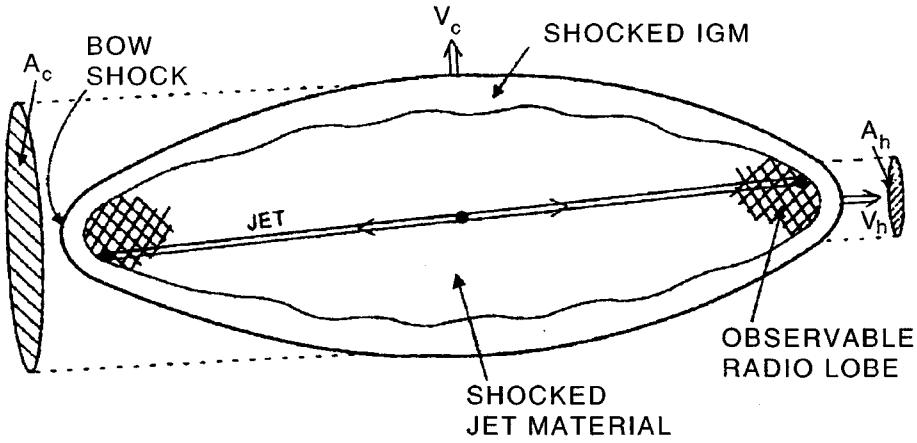

Fig. 3. – Formation of extended cocoons in radio galaxies.

Jet collimation is easier when the whole body of radio galaxies is embedded in an overpressured region. The transverse dimensions of the lobes are related to the jet kinetic luminosity, and are made wide through wave propagation.

5·3. *Numerical simulations of extended lobes.* – The pioneering work in numerical simulations was produced by Norman *et al.* [42] and revealed the basic features and components discussed above. Several new features were included in later works, as intermittency in the jet thrust, jitter in the launch direction, influence of external medium (confined and free jets), relativistic effects and radiative losses.

The formation of overpressured cocoons and the substantial stability of supersonic jets were confirmed, although numerical simulations are still affected by the limitations in Reynolds number and calculated domain. Hot spots were connected with Mach disks and knots with internal shocks.

Concerning the influence of the external medium, light jets ($\rho_j/\rho_{ext} < 1$) are surrounded by an overpressured inflating region, the cocoon, while heavy jets ($\rho_j/\rho_{ext} \geq 1$) are naked and do not mix with external gas. Relativistic jets display a phenomenology similar to classical non-relativistic jets, but propagate more efficiently into the external medium following a law [43]:

$$v_h = \frac{v_j}{1 + \sqrt{\nu}\,[1 - (V_j/c)^2]^{1/2}}.$$

Finally, thermal radiative cooling develops dense cool shells at the working surface of jets and decreases the number and strength of internal shocks [44]. Instead, in non-thermal synchrotron radiative losses do not affect the overall phenomenology, but simply slow down the dynamical evolution of instabilities and turbulent mixing.

Fully *3D hydro simulations* show that the morphology of radio lobes is dominated by 3D effects [39, 42, 45, 46]. The main results are:

- strong turbulent mixing between jet and ambient material occurs, characterized by small scale vortices, while in 2D simulations large scales were dominant, therefore the jet is more efficiently protected from disruption than in 2D results;
- the usual sequence of oblique internal shocks appears;
- mixing does not reach the very backbone of the jet;
- instead of the Mach disk now a less defined termination shock accomplishes the transition to the subsonic flow and bow shock;
- the cocoon ends up to be overdense;
- jets display a vigorous "flapping" of their heads;
- the lack of concentration in the jet head thrust slows down the working surface advancement speed to about half of the analytic estimates.

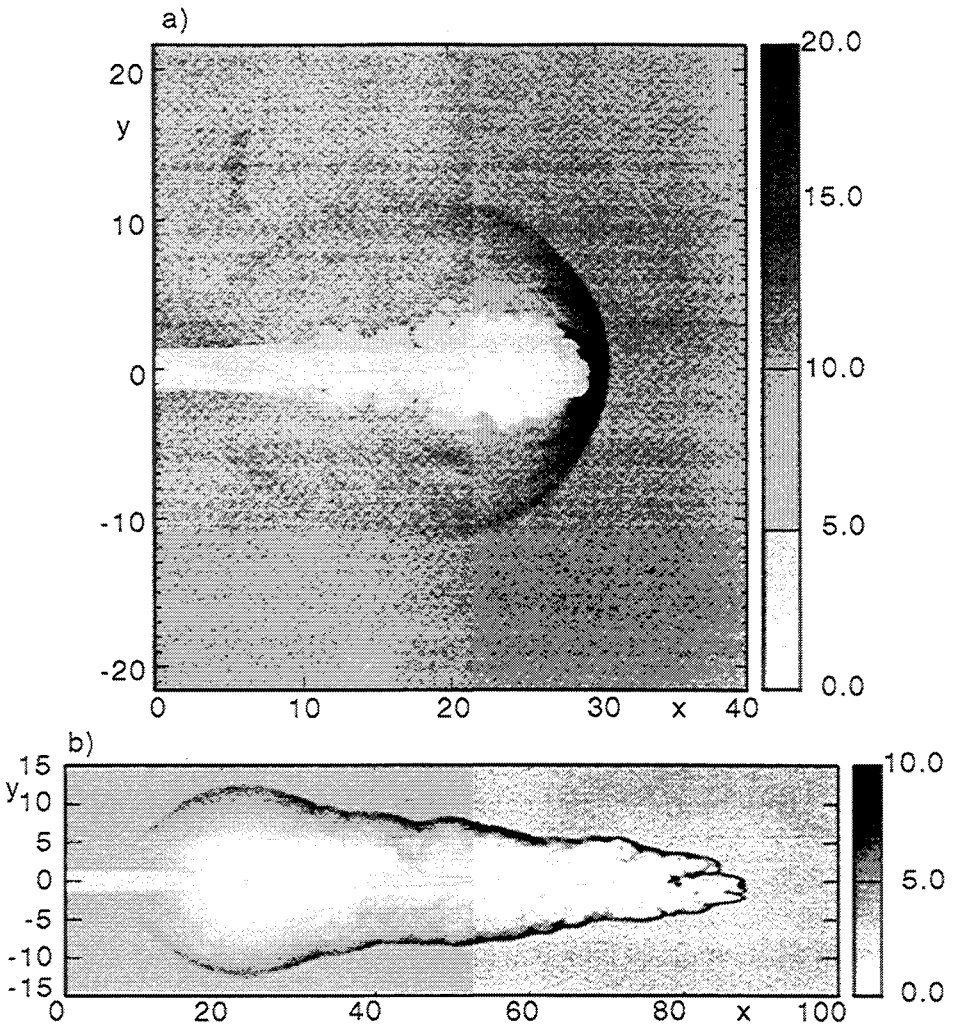

Fig. 4. – Morphologies of extended cocoons from numerical simulations. a) Low Mach number; b) high Mach number and light jets.

Effects of magnetic fields have been studied in the ideal MHD limit. Poloidal fields make the flow resemble the purely hydro simulations displaying filaments, knots and hot spots, but smaller cocoons and slower head advancement [47]. Azimuthal fields confine the plasma through a radial $\mathbf{J} \times \mathbf{B}$ force and do not allow the formation of large cocoons, because backflow and return current are constrained to the very surface of the jet [46,48]. The shocked material at the working surface accumulates in a protruding "nose" because the radial current at the Mach disk gives rise to a forward longitudinal $\mathbf{J} \times \mathbf{B}$ force.

We show in fig. 4 an example of the results of a 3D hydro simulation performed with a PPM code to study the long term dynamics of the jet/ambient interaction for an extensive parameter space towards high Mach numbers and for light jets [39]. The phases of evolution are dominated by the unfolding of instabilities at the discontinuities between jet and external material. The numerical simulations allow to follow the formation of shocks at the leading front and the development of ripple instabilities that compress the

jet behind its head giving rise to the series of conical internal shocks.

The dynamics depends essentially on M_j: a stronger interaction between biconical shocks and jet head is obtained for high Mach number jets. The dependence on $\nu = \rho_\mathrm{ext}\rho_\mathrm{j}$ is relatively weak for light jets.

The *jet thrust* is modulated by the biconical shocks behind the head and can produce a recurrent acceleration of the head by localized compressions. In fact one finds two classes of dynamical evolution:

1. jets with high M_j and ν have faster v_h and show recurrent acceleration phases as due to strong thrust by the biconical shocks;

2. jets with low M_j and ν have slower v_h as the shock thrust is weak.

The critical parameter is the inclination angle of the biconical shocks that determines the thrust behind the head: oblique shocks must have a small inclination angle on the axis in order to produce a strong acceleration effect.

The dynamics of the cocoon arising from the backflow follows the head's features, but the influence of the density contrast is stronger. One can have:

1. spear-headed cocoons (fig. 4b), bearing the sign of the recurrent acceleration of jets with high M_j; these morphologies characterize high luminosity radio sources, such as 3C42, 3C184.1, 3C223, 3C349, 3C390.3 [49];

2. fat cocoons (fig. 4a), more extended laterally; shocks form only in the frontal part of the cocoon, as in sources like 3C296 and 3C173.1.

In conclusion, jets are typically light with respect to the external medium if they have large cocoons, and slow jets correspond to the largest cocoons.

REFERENCES

[1] REES M. J., *Nature*, **229** (1971) 312.
[2] SCHEUER P. A. G., *Mon. Not. R. Astron. Soc.*, **166** (1974) 513.
[3] BLANDFORD R. D. and REES M. J., *Mon. Not. R. Astron. Soc.*, **169** (1974) 395.
[4] BURBIDGE G. R., *Astrophys. J.*, **129** (1958) 841.
[5] FERRARI A., *Annu. Rev. Astron. Astrophys.*, **36** (1998) 539.
[6] PARKER E. N., *Interplanetary Dynamical Processes* (Interscience) 1963.
[7] FERRARI A., TRUSSONI E., ROSNER R. and TSINGANOS K., *Astrophys. J.*, **294** (1985) 397.
[8] TSINGANOS K., SAUTY C., SURLANTZIS G., TRUSSONI E. and CONTOPOULOS J., *Solar and Astrophysical MHD Flows* (Kluwer) 1996, p. 427.
[9] BLANDFORD R. D. and PAYNE D. G., *Mon. Not. R. Astron. Soc.*, **199** (1982) 883.
[10] PELLETIER G. and PUDRITZ R. E., *Astrophys. J.*, **394** (1992) 117.
[11] CAMENZIND M., *Astrophysical Jets - Open Problems* (Gordon and Breach) 1998, p. 3.
[12] GOLDREICH P. and JULIAN W. H., *Astrophys. J.*, **157** (1969) 869.
[13] BLANDFORD R. D., *Mon. Not. R. Astron. Soc.*, **176** (1976) 465.
[14] LOVELACE R. V. E., *Nature*, **262** (1976) 649.

[15] BLANDFORD M. D. and ZNAJEK R. L., *Mon. Not. R. Astron. Soc.*, **179** (1977) 433.
[16] MACDONALD D. and THORNE K. S., *Mon. Not. R. Astron. Soc.*, **188** (1982) 345.
[17] PHINNEY E. S., *Astrophysical Jets* (Reidel) 1982, p. 201.
[18] PUNSLY B. and CORONITI F. V., *Astrophys. J.*, **350** (1996) 518.
[19] BLANDFORD R. D. and BEGELMAN M., *Mon. Not. R. Astron. Soc.*, **303** (1999) L1.
[20] NOBILI L., *Astrophysical Jets - Open Problems* (Gordon and Breach) 1998, p. 31.
[21] GHISELLINI G., BODO E., TRUSSONI E. and REES M. J., *Astrophys. J.*, **362** (1990) L1.
[22] UCHIDA Y. and SHIBATA K., *Publ. Astron. Soc. Jpn.*, **37** (1985) 515.
[23] SHIBATA K. and UCHIDA Y., *Publ. Astron. Soc. Jpn.*, **42** (1990) 39.
[24] STONE J. M. and NORMAN M. L., *Astrophys. J.*, **43** (1994) 746.
[25] MATSUMOTO R., UCHIDA Y., HIROSE S., FERRARI A. *et al.*, *Astrophys. J.*, **461** (1996) 115.
[26] ROMANOVA M. M., USTYUGOVA G. V., KOLDOBA A. V., CHECHETKIN V. M. and LOVELACE R. V. E., *Astrophys. J.*, **482** (1997) 708.
[27] OUYED R. and PUDRITZ R. E., *Astrophys. J.*, **482** (1997) 712; **484** (1997) 794.
[28] HEYVAERTS J. and NORMAN C., *Astrophys. J.*, **1989** (347) 1045.
[29] MEIER D. L., EDGINGTON S., GODON P., PAYNE D. G. and LIND K. R., *Nature*, **388** (1997) 350.
[30] THOMPSON P. A., *Compressible Fluid Dynamics* (McGraw-Hill) 1972.
[31] FERETTI L., FANTI R., PARMA P., MASSAGLIA S., TRUSSONI E. and BRINKMANN W., *Astron. Astrophys.*, **298** (1995) 699.
[32] FERRARI A., ROSNER. R., TRUSSONI E. and TSINGANOS K., *Astrophys. J.*, **300** (1986) 577.
[33] DE YOUNG D., *Astrophys. J.*, **241** (1980) 81.
[34] APPL S. and CAMENZIND M., *Astron. Astrophys.*, **274** (1993) 699.
[35] BENFORD G., *Mon. Not. R. Astron. Soc.*, **183** (1978) 29.
[36] BROWN G. L. and ROSHKO A., *J. Fluid Mech.*, **284** (1974) 171.
[37] GERWIN R. A., *Rev. Mod. Phys.*, **40** (1968) 652.
[38] ROSSI P., BODO G., MASSAGLIA S. and FERRARI A., *Astrophys. J.*, **414** (1993) 112.
[39] BODO G., ROSSI P., MASSAGLIA S., FERRARI A., MALAGOLI A. and ROSNER R., *Astron. Astrophys.*, **333** (1998) 1117.
[40] KUNDT W., *Jets from Stars and Galactic Nuclei* (Springer Verlag) 1996.
[41] CIOFFI D. F. and BLONDIN J. M., *Astrophys. J.*, **392** (1992) 458.
[42] NORMAN M. L., *ASP Conf. Ser.*, **100** (1996) 319.
[43] MARTÍ J. MA., MÜLLER E. and IBANEZ J. MA., *Astrophys. J.*, **448** (1995) L105.
[44] MASSAGLIA S., BODO G. and FERRARI A., *Astron. Astrophys.*, **307** (1996) 997.
[45] ARNOLD C. N. and ARNETT W. D., *Astrophys. J.*, **1986** (305) L57.
[46] CLARKE D. A., *ASP Conf. Ser.*, **100** (1996) 311.
[47] KÖSSL D., MULLER E. and HILLEBRANDT W., *Astron. Astrophys.*, **229** (1990) 378.
[48] LIND K. R., PAYNE D. G., MEYER D. L. and BLANDFORD R. D., *Astrophys. J.*, **344** (1989) 89.
[49] LEAHY J. P. and PERLEY R. A., *Astrophys. J.*, **344** (1991) 89.